Interannual variations and trends in global land surface phenology derived from enhanced vegetation index during 1982–2010

Xiaoyang Zhang, Bin Tan & Yunyue Yu

International Journal of Biometeorology

ISSN 0020-7128

Int J Biometeorol
DOI 10.1007/s00484-014-0802-z

Springer

Int J Biometeorol
DOI 10.1007/s00484-014-0802-z

Interannual variations and trends in global land surface phenology derived from enhanced vegetation index during 1982–2010

Xiaoyang Zhang · Bin Tan · Yunyue Yu

Received: 7 April 2013 / Revised: 31 January 2014 / Accepted: 15 February 2014

Abstract Land surface phenology is widely retrieved from satellite observations at regional and global scales, and its long-term record has been demonstrated to be a valuable tool for reconstructing past climate variations, monitoring the dynamics of terrestrial ecosystems in response to climate impacts, and predicting biological responses to future climate scenarios. This study detected global land surface phenology from the advanced very high resolution radiometer (AVHRR) and the Moderate Resolution Imaging Spectroradiometer (MODIS) data from 1982 to 2010. Based on daily enhanced vegetation index at a spatial resolution of 0.05 degrees, we simulated the seasonal vegetative trajectory for each individual pixel using piecewise logistic models, which was then used to detect the onset of greenness increase (OGI) and the length of vegetation growing season (GSL). Further, both overall interannual variations and pixel-based trends were examined across Koeppen's climate regions for the periods of 1982–1999 and 2000–2010, respectively. The results show that OGI and GSL varied considerably during 1982–2010 across the globe. Generally, the interannual variation could be more than a month in precipitation-controlled tropical and dry climates while it was mainly less than 15 days in temperature-controlled temperate, cold, and polar climates. OGI, overall, shifted early, and GSL was prolonged from 1982 to 2010 in most climate regions in North America and Asia while the consistently significant trends only occurred in cold climate and polar climate in North America. The overall trends in Europe were generally insignificant. Over South America, late OGI was consistent (particularly from 1982 to 1999) while either positive or negative GSL trends in a climate region were mostly reversed between the periods of 1982–1999 and 2000–2010. In the Northern Hemisphere of Africa, OGI trends were mostly insignificant, but prolonged GSL was evident over individual climate regions during the last 3 decades. OGI mainly showed late trends in the Southern Hemisphere of Africa while GSL was reversed from reduced GSL trends (1982–1999) to prolonged trends (2000–2010). In Australia, GSL exhibited considerable interannual variation, but the consistent trend lacked presence in most regions. Finally, the proportion of pixels with significant trends was less than 1 % in most of climate regions although it could be as large as 10 %.

Keywords Long-term global phenology · Interannual variation · Trend · Remote sensing

X. Zhang (✉)
Geospatial Sciences Center of Excellence (GSCE), South Dakota State University, 1021 Medary Ave., Wecota Hall 506B, Brookings, SD 57007-3510, USA
e-mail: xiaoyang.zhang@sdstate.edu

B. Tan
Earth Resources Technology Inc. at NASA Goddard Space Flight Center, Code 614.5, Greenbelt, MD 20771, USA

Y. Yu
NOAA/NESDIS/STAR, 5825 University Research Ct, College Park, MD 20740, USA

Published online: 18 March 2014

Introduction

Vegetation phenology reflects a complex suite of interactions among atmospheric, biospheric, and soil biogeochemical properties. Because vegetation phenology effectively reflects climate change, the Intergovernmental Panel on Climate Change (IPCC) reported that phenology is one of the simplest and most effective indicators of climate change (IPCC 2007). Long-term observations and recording of changes in plant phenology support efforts to understand trends in regional and global climate change, to reconstruct past climate variations, to explore the magnitude of climate change impacts on

vegetation growth, and to predict biological responses to future climate scenarios.

Vegetation phenology for a specific species is widely observed in fields. Crop calendars have been used in agriculture for thousands of years in China (Zhu and Yuan 1963), and phenological records have a history going back to the early 1700 s in Europe (e.g., Sparks and Carey 1995) and to the 1800 s in Japan (Lauscher 1978). Recently, several networks of field phenological observations have been established worldwide to record phenological events distributed spatially across a regional area. These networks include PlantWatch in Canada, the National Phenology Network (NPN) in the USA (United States of America), the European Phenology Network, the Japan Phenological Eyes Network (PEN), and the UK (United Kingdom) Phenology Network. These networks record the timing of species-specific events. More recently, a network of "phenocams" has been established in North America (NA), which currently includes more than 50 sites (Richardson et al. 2009). The phenocams observe the seasonality of plant canopy in the field from digital webcams, which provide "near-surface" remotely sensed vegetation indices and have the potential to provide a rich source of quantitative data related to phenology at daily time scales.

Throughout the last 3 decades, satellite remote sensing has become a widely used mechanism for monitoring phenology in vegetation communities, which is referred to as land surface phenoloy (LSP) (de Beurs and Henebry 2004; Friedl et al. 2006). To detect long-term ecosystem variation and climate change at regional and global scales, LSP has been commonly retrieved from time series of the normalized difference vegetation index (NDVI) from the advanced very high resolution radiometer (AVHRR), the VEGETATION instrument onboard the SPOT spacecraft, and the Moderate Resolution Imaging Spectroradiometer (MODIS) onboard NASA's Terra and Aqua spacecraft. AVHRR dataset, available since July 1981, provides the longest daily global observations and is commonly used for detecting land surface change at local and global scales. Different calibration methods generate several AVHRR NDVI datasets. NASA's Global Inventory Modeling and Mapping Studies (GIMMS) group produced a global NDVI dataset at a resolution of biweekly 8 km from 1981 to 2011 (Tucker et al. 2005). NASA/NOAA Pathfinder AVHRR Land (PAL) provided a global 10-day composite of 8-km NDVI, which spans from July 1981 to December 1999 (James and Kalluri 1994). The USGS (US Geological Survey) EROS Data Center generated a 10-day composite of 1-km AVHRR NDVI for the contiguous USA since 1989 (Eidenshink 1992). NOAA NESDIS (National Environmental Satellite, Data, and Information Service) developed a weekly 4-km global vegetation index (GVIx) product from 1981 to present (Kogan et al. 2003). The latest dataset is the Long Term Data Record (LTDR), which is designed to produce a consistent long-term record from the AVHRR and MODIS sensors (Pedelty et al. 2007). The AVHRR LTDR provides daily 0.05° (~5 km) reflectance data from 1981 to 1999.

The time series of NDVI data has been extensively used for detecting phenological trend and interannual variation. AVHRR NDVI data have been commonly applied to retrieve the start and end of vegetation growth using a number of methods including NDVI threshold (Lloyd 1990; Fisher 1994; Myneni et al. 1997), middle point (White et al. 1997), moving average (Reed et al. 1994), growing-degree-day-based NDVI model (de Beurs and Henebry 2004), Gaussian function (Jönsson and Eklundh 2002), and curvature change rate (Zhang et al. 2007). Analyzing long-term AVHRR-derived phenology has revealed an early trend in spring events and a late trend at the end of the growing season in middle–high latitudes (e.g., Myneni et al. 1997; Tucker et al. 2001; Zhou et al. 2001; de Beurs and Henebry 2005a; Chen et al. 2005; Delbart et al. 2005; Piao et al. 2006; Zhang et al. 2007; Julien and Sobrino 2009; de Jong et al. 2011). The shift rate varies with different AVHRR time periods and research approaches, ranging from 0.1 to 0.8 days/year in spring events and 0.1 to 1.1 days/year in growing season length. However, the late spring trend has also been found in southern NA from 1982 to 2005 (Zhang et al. 2007) and in boreal forests from 1993 to 2004 (Delbart et al. 2005). In contrast, it has been found that spring vegetation growth generally shows no significant trend from 1982 to 2006 over NA (Reed 2006; White et al. 2009).

This study investigated interannual LSP variation using a daily enhanced vegetation index which was calculated from the AVHRR LTDR and the MODIS Climate Modeling Grid (CMG) records during 1981–2010. The temporal trajectory of the vegetation index was simulated using piecewise logistic models for land surface phenology detection after satellite data quality was explicitly employed. Further, phenological trend and interannual variation in both greenup onset and growing season length (GSL) were examined across Koeppen's climate regions in each continent, respectively.

Methodology

Long-term daily vegetation index

The enhanced vegetation index (EVI), calculated from reflectance in blue, red, and near-infrared bands, has advantages over NDVI in quantifying vegetation activity (Huete et al. 2002). It reduces sensitivity to soil, nonphotosynthetically active vegetation (i.e., litter and woody tissues), and atmospheric effects but still remains sensitive to variation in canopy density where NDVI becomes saturated (Huete et al. 2002; Rocha et al. 2008).

Recently, a two-band EVI (EVI2) has been proposed, which is calculated from red and near-infrared reflectances (Huete et al. 2006; Jiang et al. 2008). EVI2 remains functionally equivalent to EVI but can be derived from satellite sensors without blue band, such as AVHRR. Thus, EVI2 could be used to monitor vegetation phenology and activity across a variety of ecosystems over a long-time period (Rocha and Shaver 2009).

A long-term dataset of global EVI2 has been generated from the daily land surface reflectance in the AVHRR LTDR and the MODIS CMG records. The AVHRR LTDR (1981–1999) was produced by a NASA-funded REASoN project (Pedelty et al. 2007). It aims to produce a multidecade time series of reliable data from several sensors during the 1980s and 1990s, compatible with data retrieved from MODIS. The LTDR (version 3) processes Global Area Coverage (GAC) data using the following approaches: (1) radiometric corrections were processed using ocean-clouds vicarious calibration algorithm (Vermote and Kaufman 1995), in which the independently derived sets of AVHRR calibration coefficients were consistent with an accuracy of 1 %; (2) viewing and illumination were adjusted using Bidirectional Reflectance Distribution Function (BRDF) techniques; (3) rigorous cloud and cloud shadow were screened using Cloud Advanced Very High Resolution Radiometer (CLAVR-1) (Stowe et al. 1999); and (4) water-vapor observation was corrected using reanalysis data from the NOAA NCEP. As a result, the LTDR dataset (version 3) consists of daily data including information from AVHRR channels 1 to 5, as well as ancillary data describing sun-sensor-target geometry at a spatial resolution of 0.05° (~5 km), which is the same as MODIS Climate Modeling Grid (CMG) products (since 2000) (http://ltdr.nascom.nasa.gov/cgi-bin/ltdr/ltdrPage.cgi?fileName=MODIS2LTDR).

A long-term data record of spectral vegetation index (VI, which are NDVI and EVI2) from both AVHRR LTDR and MODIS CMG was later generated with the support of a NASA MEaSUREs project. To merge VI from multiple-sensor data, data continuity and compatibility have been scientifically investigated. Analysis of AVHRR GAC broader band observations and Terra MODIS CMG narrower bands, which are simulated from Hyperion data, has demonstrated capability in combining EVI2/NDVI from different sensors (Kim et al. 2010). Because NOAA-14 AVHRR from 2000 to 2001 is not recommended for scientific uses due to significant orbital drift, there is no overlapping period of observations between AVHRR LTDR and MODIS CMG. Thus, SPOT-4 VGT was applied to bridge these two datasets (Tsend-Ayush et al. 2012). The long-term daily VI data from AVHRR and MODIS data at a spatial resolution of 0.05° were generated using a set of functions with two linear polynomials (Tsend-Ayush et al. 2012; Yoshioka et al. 2012). The VI relationship equations eliminate the soil brightness effect by utilizing the vegetation isoline equations and reduce the effects from biophysical properties by separating land cover types (Yoshioka et al. 2012). We obtained the long-term daily EVI2 over the last 30 years from the University of Arizona (http://vip.arizona.edu/viplab_data_explorer).

Detection of vegetation phenology

To establish a long-term record of global LSP from satellite data, phenological metrics are defined according to vegetation seasonal growing cycles. Briefly, a seasonal cycle of vegetation growth consists of a greenup phase, a maturity phase, a senescent phase, and a dormant phase (Zhang et al. 2003). These four phases are characterized using four phenological transition dates in the time series of greenness data: (1) greenup onset, the date of onset of greenness increase (OGI); (2) maturity onset, the date of onset of greenness maximum; (3) senescence onset, the date of onset of greenness decrease; and (4) dormancy onset, the date of onset of greenness minimum. Furthermore, GSL is defined as the time difference between greenup onset and dormancy onset.

To identify the global phenological metrics, we used a piecewise-logistic-model-based LSP detection algorithm (PLM-LSPD, Zhang et al. 2003). This PLM-LSPD has been demonstrated to be effective in depicting the seasonality of satellite greenness across various ecosystems (Zhang et al. 2003, 2006). This was then applied to investigate seasonal vegetation growth using webcam data (Richardson et al. 2006; Kovalskyy et al. 2012), Landsat TM data (e.g., Fisher et al. 2006; Kovalskyy et al. 2012), AVHRR data (e.g., Zhang et al. 2007; Julien and Sobrino 2009), and MODIS data (e.g., Zhang et al. 2003, 2006; Ahl et al. 2006; Liang et al. 2011). Thus, the PLM-LSPD is believed to be applicable for the detection of long-term global vegetation phenology from EVI2 data.

Here, we briefly introduce the PLM-LSPD for processing temporal EVI2 data for phenology detection. First, we smoothed the time series of EVI2 based on the following assumptions: (1) vegetation growth is a continuous process without sharp increases or decreases, (2) the time between successive peaks in separate vegetation growth cycles is longer than 3 months in forests and longer than 2 months for other plant functional types, (3) the magnitude of EVI2 values is generally lowered by contamination from clouds and atmosphere, and (4) a single isolated maximum in EVI2 value in a time series is not always reliable. To reduce the data size and computation time, we first generated a 3-day composite dataset from daily EVI2 data by selecting the best quality data and using the maximum value composite. We then removed the observations of clouds and snow cover from temporal EVI2 data. The cloud and snow covers are described in the quality assurance flag in the LTDR and MODIS CMG datasets. Additionally, the background EVI2 value at each pixel, which represents the minimum EVI2 consisting of soil and seasonally stable vegetation in an annual time series

(Zhang et al. 2007), was identified and used to replace EVI2 values that varied irregularly during a winter period. The data gaps caused by clouds were filled by linear interpolation using neighboring good quality data. The time series of EVI2 data at each pixel was finally smoothed using a Savitzky-Golay filter and a running local median filter.

EVI2 time series in a growing phase (EVI2 consistent increase) and a senescent phase (EVI2 consistent decrease) was modeled using a logistic function, respectively. Phenological transition dates within each growth or senescence phase were identified using the rate of change in the curvature of the modeled curves. Specifically, transition dates correspond to the day of year (DOY) on which the rate of change in curvature in the EVI2 data exhibits local minima or maxima (Zhang et al. 2003). Note that if the annual variation in EVI2 was subtle (<0.04), such as in some evergreen forests and shrublands, phenological metrics were not retrieved. Moreover, if the annual EVI2 time series was very flat in some shrublands, the curvature change rate might produce a very early timing of greenup onset. In this case, a 5 % threshold was used to determine the start and the end of a growing season.

GSL was calculated using the difference between the timing of greenup onset and dormancy onset. This was straightforward in the regions where vegetation generally grew from spring to autumn within a calendar year. For the regions where a growing cycle spanned 2 different calendar years, GSL was assigned to the year that greenup onset occurred.

Determination of the quality of an annual time series EVI2

The accuracy of phenology detection is strongly dependent on the quality of time series EVI2 data. A smooth approach could reduce some of the uncertainties, but missing observations in the time series greatly reduce the detection precision of phenologic metrics (Zhang et al. 2009). We used the proportion of good quality observations (*Pqa*) during a vegetation growing season (the time period between greenup onset and dormancy onset) to evaluate the phenology detections:

$$Pqa = Nqa/T$$

where T is the total number of 3-day EVI2 during a growing season, and Nqa is the number of good quality observations within a vegetation growing season. An EVI2 is counted as one good observation if there is one good value within a moving window of three 3-day EVI2. This is due to the fact that the error in phenology detection is small if the annual greenness cycle is simulated using a logistic model from EVI2 data with the temporal resolution finer than 8 days (Zhang et al. 2009).

Investigation of trend and interannual variation in phenology

The trend and interannual variation in both OGI and GSL were analyzed across the globe. This analysis was performed based on climate regions respectively in each continent. This was due to the fact that the magnitude and rate of climate change primarily vary with climate regions which are commonly classified based on monthly temperature and precipitation and that climate change can be effectively indicated by the variation in vegetation phenology. In other words, if the climate variables change within a climate region, vegetation phenology would vary correspondingly, although phenological timing could vary with vegetation types. To examine phenological variation in a regional or local area, ecoregion or phenoregion could provide localized patterns because ecoregions distinguish areas that share common climatic characteristics and then vegetation properties (Olson et al. 2001), and phenoregions characterize seasonal variation in NDVI and climatology (White et al. 2005; Hargrove et al. 2009). However, in investigating the overall variation in long-term phenology across the globe, it is assumed that the phenological variation in climate regions across various geographic areas could reflect the general pattern of climate change. Therefore, we first stratified both OGI and GSL by geographic regions and climatic classes, respectively (Fig. 1). The geographic regions were divided into North America (NA), South America (SA), Europe (EU), Asia (AS), Australia (AU), Northern Hemisphere of Africa (NAF), and Southern Hemisphere of Africa (SAF). The climatic classes, selected from Koeppen's climate classification, were developed by the FAO-SDRN Agrometeorology group (http://www.fao.org/nr/climpag/globgrids/KC_classification_en.asp, 2006) (Fig. 1). This system consists of the following classes: (1) tropical climate—fully humid season (Af), monsoon type (Am), dry summer (As), and dry winter (AW); (2) dry climate—steppe climate (BS) and desert climate (BW); (3) temperate climate—fully humid season (Cf), dry winter (Cw), and dry summer (Cs); (4) cold climate—fully humid season (Df), dry winter (Dw), and dry summer (Ds); and (5) polar climate—tundra (ET) and frost climate (EF).

The time series of OGI and GSL was finally applied to detect the trends for each climate region using a linear regression model. The trends were calculated for the two periods of 1982–1999 and 2000–2010, separately. This was due to the fact that phenology from 1982 to 1999 was derived from AVHRR data which were widely used for phenological trend detection in previous studies. In contrast, phenology from 2000 to 2010 was detected from MODIS data, which have better quality because MODIS land spectral bands were explicitly designed for land surface monitoring (Justice et al. 1997). Moreover, we found that the inconsistency between AVHRR LTDR and MODIS CMG still remains in some regions although great efforts have been exerted to continue

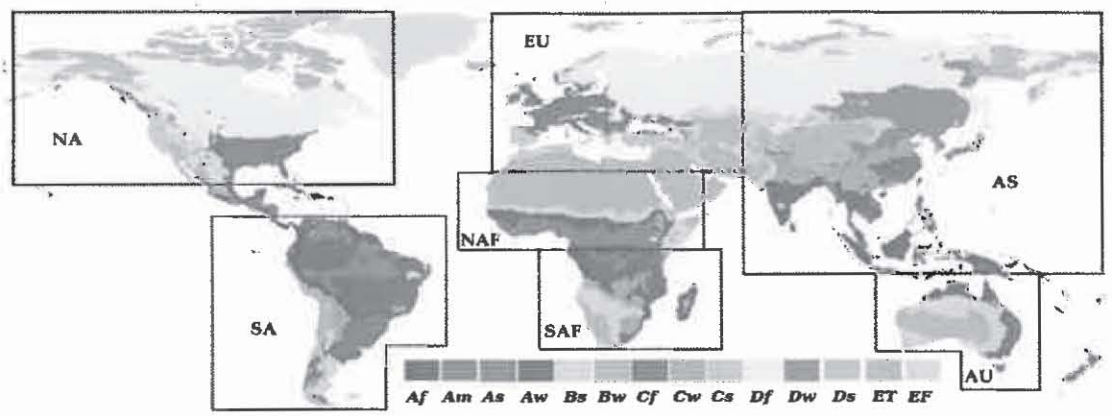

Fig. 1 Koeppen's climate classification (based on FAO-SDRN Agrometeorology group, 2006) and geographic regions

these two datasets. Such sensor inconsistency could significantly affect trend analysis (de Beurs and Henebry 2005b).

In each time period, we calculated overall trend and pixel-based trend in a climate region, separately, after the geographic projection (0.05°) was reprojected to the Goode homolosine projection (an equal-area project) at a spatial resolution of 5 km. The overall trend was calculated from a time series of average phenological values in a region. The pixel-based trend was used to determine the pixels with significantly positive and negative trends and the corresponding proportion of pixels (area) in a climate region. Crop land was excluded in this analysis because crop phenology is controlled by human activities. This data processing allowed us to understand well both the overall changes and the percentage of changing pixels that were significantly affected by climate change within a climate region.

Results

Quality of annual time series of EVI2

Reliable phenology retrieval is strongly dependent on the quality of annual time series of satellite observations. Figure 2 presents the spatial pattern of the average percentage of good quality observations. Overall, the percentage of good observations was much higher in MODIS observations (2000–2010) than in AVHRR observations (1982–1999). In MODIS observations, the percentage of good observations during a vegetation growing season was generally larger than 75 % except in tropical climates, England, and northwestern NA. In contrast, good observations from AVHRR data were less than 75 % in most regions except for dry climates. However, good observations were less than 50 % in large parts of Western Europe, East Asia, the Amazon basin, and West Africa (Fig. 2). This is due to the fact that MODIS CMG data were aggregated from 500-m pixels with high quality. In contrast, AVHRR LTDR was generated from 4-km pixels which were sampled onboard the satellite by selecting every third 1-km local area coverage (LAC) data line, four of every five samples along this line, and averaging these data.

Interannual variation in the onset of greenness increase

Figure 3 shows the global climatology of the onset of greenness increase from 1982 to 2010. The spatial pattern in OGI reflects both broad-scale variations in controlling mechanisms related to climate and more local factors related to land cover and human activities (Fig. 3a). Specifically, OGI spatially shifted along latitude from 30°N northward. Zonal patterns indicate that OGI varied at a rate of 2–3 days per degree of latitude in NA, Europe, and Asia. This rate of northward progression is similar to Hopkins' law (1938; Reader et al. 1974). In NA, OGI shifted from late February in southern USA, April in northern USA, and to the end of June in the northern tundra. The dependence on latitude was spatially interrupted by elevation and human activities. The elevation effect was pronounced in large mountains such as the Himalayas in Asia, the Alps in Europe, and the Appalachians in America. Moreover, OGI in agricultural lands was frequently distinct from that of surrounding natural vegetation because of the controls applied by human management. This was highly evident in central NA, where OGI occurred much later in the Mississippi River valley and the midwestern agricultural heartland, relative to the surrounding natural vegetation.

OGI pattern was generally complex and irregular in dry climate (arid and semiarid regions) because of the highly spatial variability in water availability. However, regular patterns in local regions were commonly found. For example, in the Northern Hemisphere of Africa (the Sahelian and sub-Sahelian regions), OGI shifted smoothly from early March at around 6.5°N to mid-October in the boundary between the Sahel and the Sahara desert (17.9°N). The shift rate was about 20 days per degree of latitude; this reflected the start of the rainy season which was controlled by the migration of the Intertropical Convergence Zone (ITCZ) (Zhang et al. 2005).

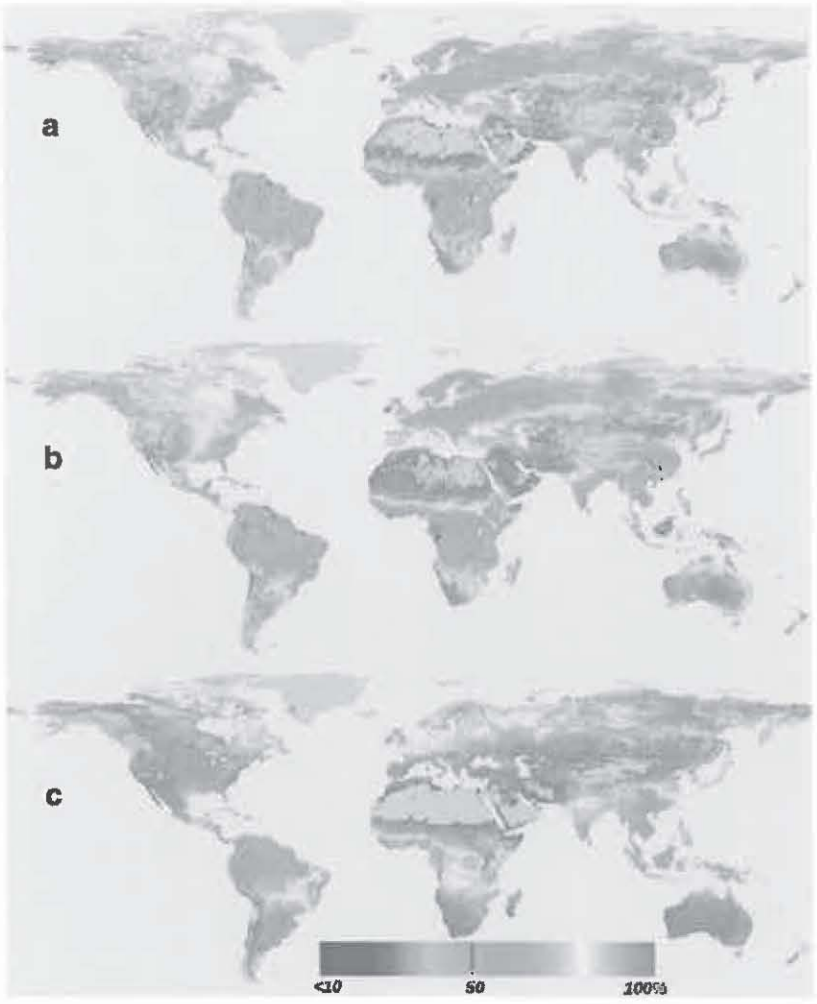

Fig. 2 Average percentages of good observations during a vegetation growing season in 1980s (**a**), 1990s (**b**), and 2000s (**c**). Note that no percentage was calculated for the pixels if no phenology was detected for any years during each period

In southern South America, green leaves emerged in the boreal summer and gradually pushed northward at a rate of about 3 days per latitude from 45° to 20°S. Along the Brazilian Highlands (in the direction from 60°W and 39°S to 35°W and 5°S), OGI shifted from July to the following February at a rate of about 0.12 days/km.

Figure 3b shows the spatial pattern in standard deviation (STD) of temporal OGI from 1982 to 2010. It reveals that STD was less than 15 days in most regions of middle–high latitude across the Northern Hemisphere, particularly across Eurasia. In contrast, STD could be larger than 40 days in tropical and subtropical regions. This is likely associated with climate forces in controlling vegetation phenology. The variance of temperature-controlled phenological timing was relatively small because seasonal temperature is generally regular among different years. However, rainfall seasonality could have large variances among different years (Lotsch et al. 2003; Zhang et al. 2010), which results in large OGI STD in water-controlled arid climate regions. In tropical rainforests, such as the Amazon, vegetation greenness phenology is affected by sunlight during the dry season (Huete et al. 2006), which leads to a large interannual variation in OGI.

Figure 4 presents interannual variation in OGI across different geographic and climate regions. Generally, OGI presented considerable interannual variability in tropical, temperate, and dry climates while it was relatively consistent in cold and polar climates. The STD of interannual OGI was generally less than 8 days in cold and polar climates and 10 days in temperate climate over the Northern Hemisphere. It was less than 21 days in tropical seasonally dry climates over the Southern Hemisphere. In dry climate, the STD was as large as 14 days in western NA, 7 days in Eurasia, 23 days in Africa, and 17 days in South America.

The overall trends in OGI showed complexity during the past 3 decades (Fig. 4 and Tables 1 and 2). In the northern tundra (ET), OGI, overall, showed an early trend at a rate of 0.25 days/year from 1982 to 1999 and 0.68 days/year from 2000 to 2010 in NA, but the early trend was not significant in both Europe and Asia. Accordingly, trend analysis of individual pixels in ET showed that the proportion of pixels was 2.2–

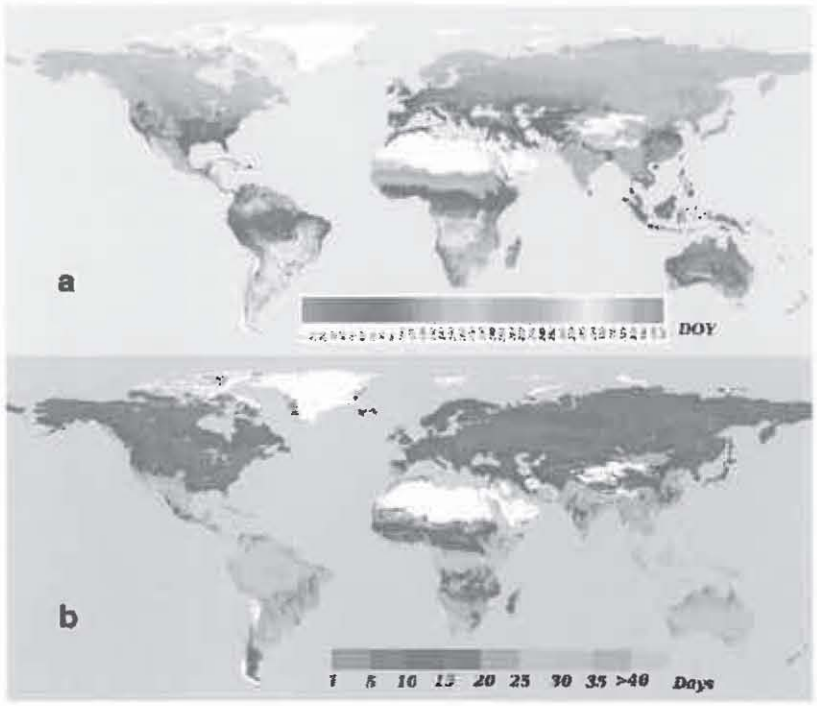

Fig. 3 Spatial pattern in OGI climatology based on data from 1982 to 2010. **a** Average of OGI and **b** standard deviation. Note that the *white color* indicates no phenology detection because of either permanent snow cover or desert

3.6 % for significantly early trends and less than 0.2 % for late trend during these two periods in NA. It was less than 0.5 % for late trend and 1.2–1.5 % for early trend in Asia, while the proportion was less than 1 % in either directions over Europe (Figs. 5 and 6).

OGI tended to be early in the cold climate of Asia and NA (Table 1). In Df climate, OGI over NA showed a significantly early shift (0.38 days/year) from 1982 to 1999 but insignificantly early shift from 2000 to 2010. No significant trend was found in either Europe or Asia. In Dw climate, which covers a large area of Asia, OGI came earlier at a significant rate of 0.22 days/year from 1982 to 1999. In contrast, OGI presented consistent early trends in Ds climate across the Northern Hemisphere although the trend was insignificant in Europe. Pixel-based trends revealed that the proportion of pixels with significantly early shifts was 10 and 6 % of the Df climate in NA from 1982 to 1999 and from 2000 to 2010, respectively, 4 and 2 % in Europe, and 5 and 3 % in Asia (Figs. 5 and 6). Accordingly, the area with significantly late shift was 1 and 2 % in NA, 5 and 7 % in Europe, and 1 and 3 % in Asia. In Dw climate, the proportion was 4 % for early shift and less than 1 % for late shift from 1982 to 1999, and it was 1–2 % in both directions from 2000 to 2010 in Asia. The proportion for significant trends was less than 0.1 % in NA and Europe, respectively.

In temperate climate, OGI showed slightly early trends in Cs from 1982 to 2010 while it became late in Cw from 2000 to 2010 over Asia. However, it presented no significant trends in both NA and Europe. At pixel level, area with either early or late trend was basically less than 1 % across the Northern Hemisphere.

In dry climate, the significant trend in OGI only occurred in BW of Asia (Table 1). It became early at a rate of 0.83 days/year from 1982 to 1999. The proportion of pixels with significant shift was less than 1 % in various regions except for BS climate (Figs. 5 and 6). In the latter, the proportion was 1.1 % (late shift from 2000 to 2010) in NA, 1.1 % (late shift from 1982 to 2010), and 1.3 % (early shift from 2000 to 2010) in Europe.

In South America, OGI mostly presented late trends during the last 3 decades (Fig. 4 and Table 2). The significantly late trend occurred in all climates from 1982 to 1999 except for Cs and ET while it only occurred in Cw from 2000 to 2010. The proportion of pixels with significantly late shift could be as large as 5 % in an individual climate region, which was much larger than that for early shift (Figs. 5 and 6).

Overall, OGI showed no significant trend in the Northern Hemisphere of Africa although early trends were transited to late trends from 1982–1999 to 2000–2010 (Table 2). However, the proportion of pixels could be as large as 3 % in a climate region, and it was generally larger for early shift than that for late shift (Figs. 5 and 6). Following the climate types, which are BW, BS, AW, and As, along latitude from northern to southern regions, the proportion for significantly early OGI shifts from 2000 to 2010 increased from 0.7 to 3.2 %, gradually. In contrast, OGI in the Southern Hemisphere of Africa mainly showed late trends. The significant trend appeared in BS, Bw, Cw from 1982 to 1999, and Cf from

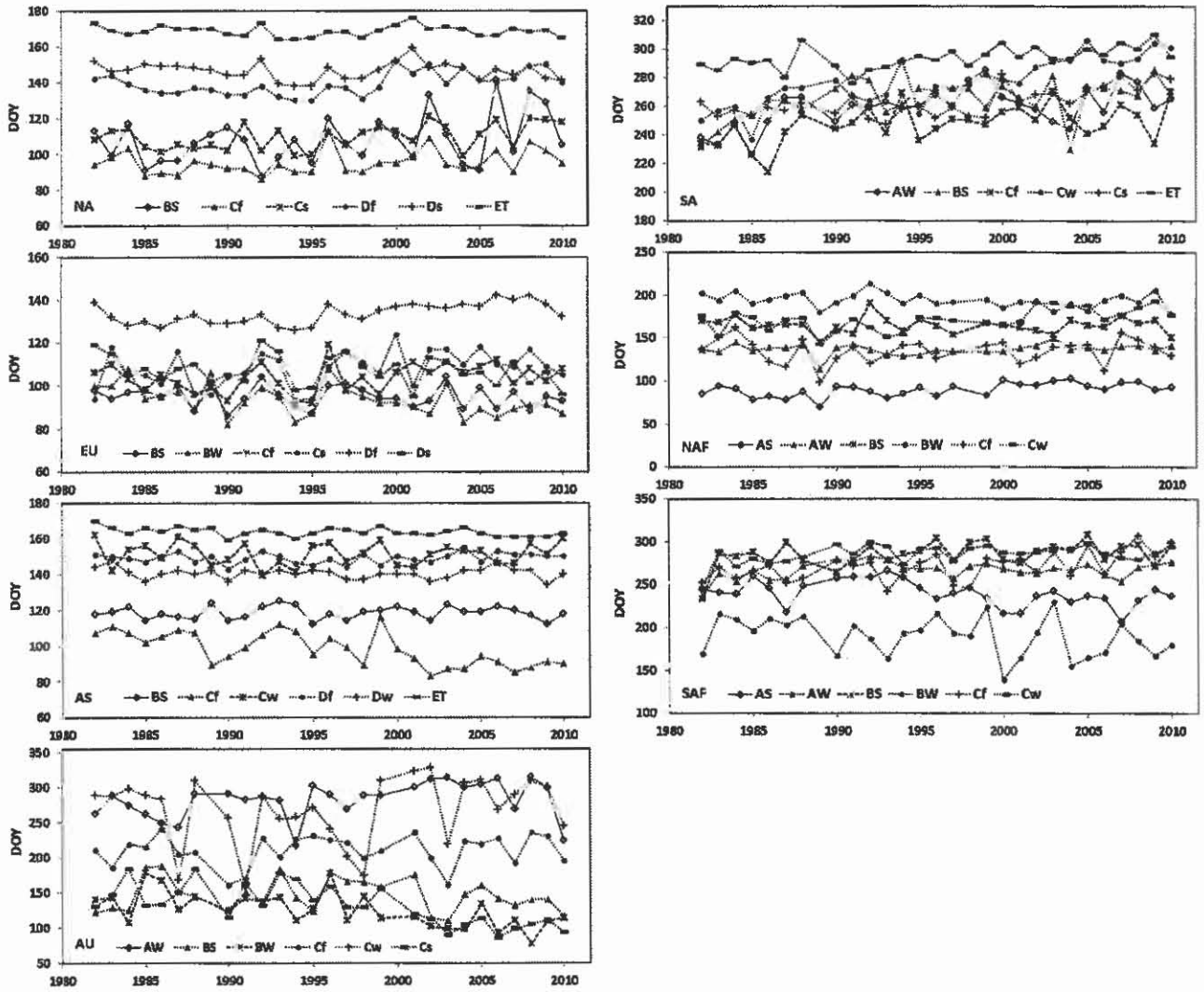

Fig. 4 Interannual variation in mean OGI across various geographic and climate regions

2000 to 2010 (Table 2). The proportion of pixels was much larger for late shift than that for early shift (Figs. 5 and 6).

In Australia, significantly early OGI trend only appeared in tropical climate (AW, 3.2 days/year) from 2000 to 2010. Pixel-based trend from 2000 to 2010 was about 4 days/year in either early or late shift with an area of 1–4.5 % in AW, BS, BW, and Cf, respectively (Figs. 5 and 6). Similar pattern appeared during the period from 1982 to 1999. Noticeably, the

Table 1 Overall trend in the onset of greenness increase (days/year) in North America (NA), Europe (EU), and Asia (AS)

OGI		AW	BS	BW	Cf	Cw	Cs	Df	Dw	Ds	ET
NA	1982–1999	N/A	0.22	−0.56	0.01	−0.36	0.08	**−0.38**	0.02	**−0.45**	**−0.25**
	2000–2010	N/A	1.20	−1.73	0.11	−1.03	0.62	−0.41	0.05	**−1.21**	**−0.68**
EU	1982–1999	N/A	−0.02	−0.35	−0.2	N/A	0.21	0.02	N/A	−0.17	0.13
	2000–2010	N/A	−0.13	−0.28	−0.31	N/A	−0.68	0.02	N/A	−0.61	−0.6
AS	1982–1999	−0.32	0.01	**−0.83**	−0.28	−0.11	**−0.41**	−0.21	**−0.22**	**−0.27**	−0.15
	2000–2010	1.24	−0.38	0.41	−0.3	**0.87**	**−0.95**	0.18	0.06	−0.39	−0.2

The bold value indicates significant trend (P value<0.1)

N/A not applicable, *OGI* onset of greenness increase, *AW* tropical climate—dry winter, *BS* dry climate—steppe climate, *BW* dry climate—desert climate, *Cf* temperate climate—fully humid season, *Cw* temperate climate—dry winter, *Cs* temperate climate—dry summer, *Df* cold climate—fully humid season, *Dw* cold climate—dry winter, *Ds* cold climate—dry summer, *ET* polar climate—tundra

Table 2 Overall trend in the onset of greenness increase (days/year) in South America (SA), the Northern Hemisphere of Africa (NAF), the Southern Hemisphere of Africa (SAF), and Australia (AU)

OGI		As	AW	BS	BW	Cf	Cw	Cs	ET
SA	1982–1999	**3.13**	**2.24**	**1.51**	**0.71**	**1.14**	**1.42**	−0.26	0.24
	2000–2010	0.72	1.09	0.82	0.57	−0.38	**2.21**	1	0.33
NAF	1982–1999	0.07	−0.36	−0.24	−0.2	−0.44	−0.11	−0.77	N/A
	2000–2010	−0.67	0.05	0.19	0.55	0.63	0.93	−0.65	N/A
SAF	1982–1999	0.02	1.16	**1.63**	**0.13**	0.29	**1.38**	**−0.18**	N/A
	2000–2010	1.22	0.55	0.78	1.37	**2.34**	−0.09	0.07	N/A
AU	1982–1999	N/A	0.97	1.19	−0.88	0.41	−3.00	−0.10	N/A
	2000–2010	N/A	**−3.18**	−2.11	−0.73	0.71	−3.16	−3.45	N/A

The bold value indicates significant trend (P value<0.1)

N/A not applicable, *OGI* onset of greenness increase, *As* tropical climate—dry summer, *AW* tropical climate—dry winter, *BS* dry climate—steppe climate, *BW* dry climate—desert climate, *Cf* temperate climate—fully humid season, *Cw* temperate climate—dry winter, *Cs* temperate climate—dry summer, *ET* polar climate—tundra

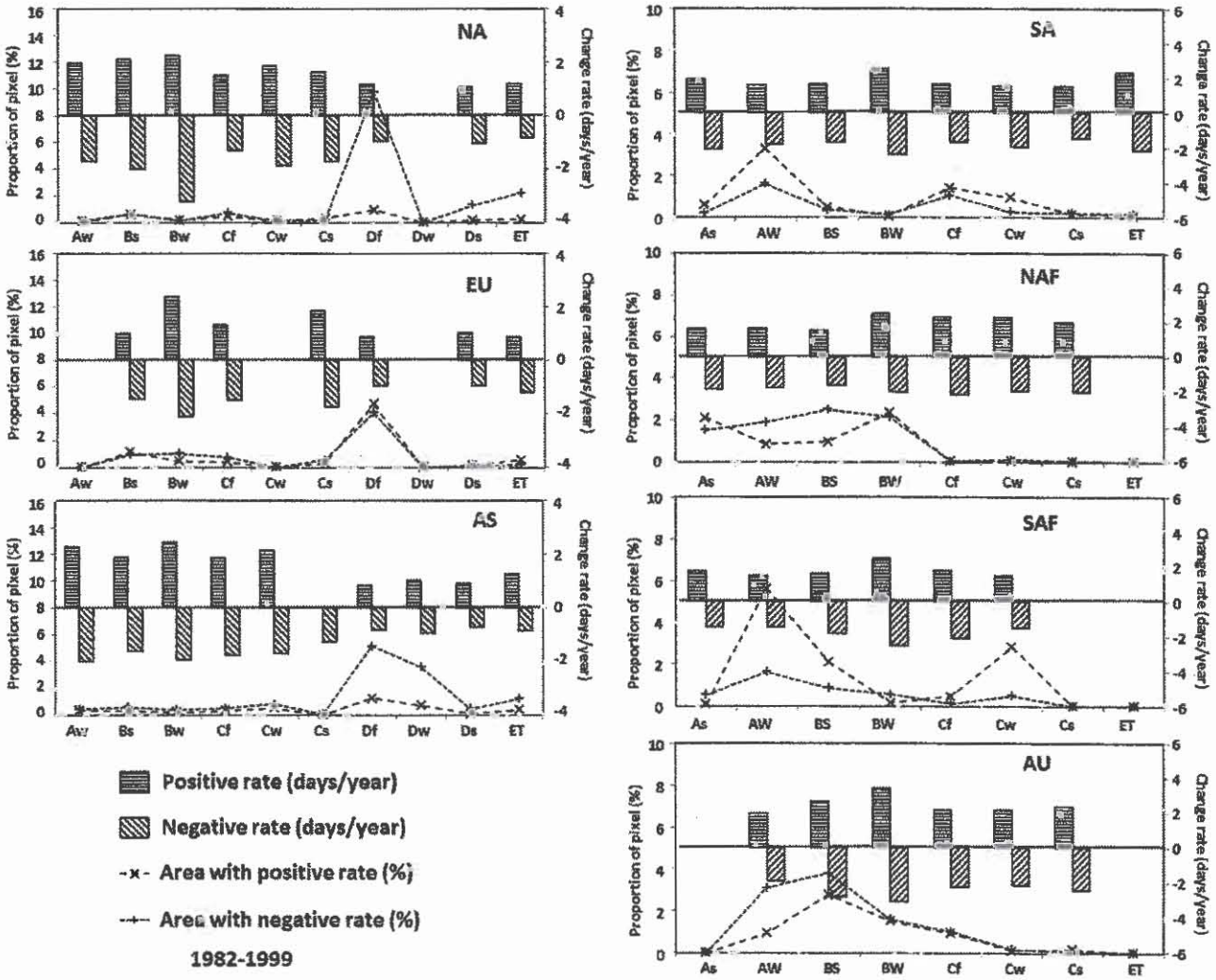

Fig. 5 The shift rate averaged from significant pixel-based trends (P <0.1) and the proportion of pixels with significant trends in greenup onset from 1982 to 1999

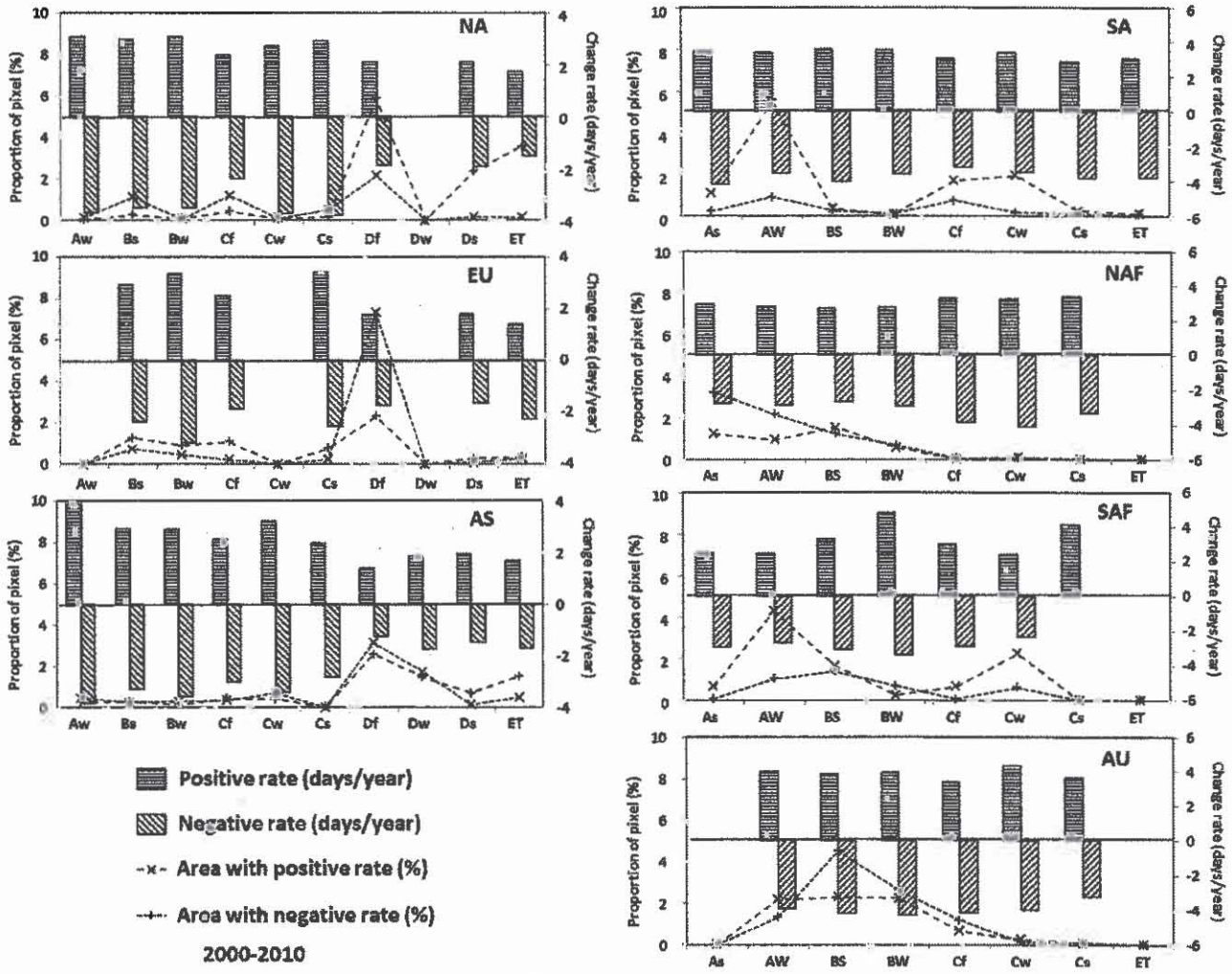

Fig. 6 The shift rate averaged from significant pixel-based trends ($P<0.1$) and the proportion of pixels with significant trends in greenup onset from 2000 to 2010

proportion for early shift was consistently large (~4 %) in BS from 1982 to 2010. Overall, OGI tended to appear earlier across the region.

Spatial pattern and interannual variation in growing season length

Figure 7 shows the spatial pattern of average GSL in the 1980s, 1990s, and 2000s, respectively. As expected, the pattern is very similar among the three periods. In the Northern Hemisphere, GSL showed a clear regular gradient along the latitude. It varied from about 50 days in the tundra area to around 300 days in temperate climate regions. Similar to the variation in OGI, the regular pattern in GSL was interrupted by human activity and elevation. Indeed, the spatial shift of GSL is also dependent on elevation. GSL varied from 220 days in Switzerland (north of the Alps) to about 90 days in the Alps Mountains and to 240 days in Italy (south of the Alps).

In the Southern Hemisphere, the spatial pattern in GSL was complex. Regular patterns appeared in local regions. For example, GSL varied from 125 days in Namibia to 260 days in Zimbabwe along a direction of southwest to northeast. It is worth noting that GSL in tropical forests could be shorter than that of other vegetation types because GSL in evergreen forests represents a cycle period from greenness increase to decrease. GSL was remarkably short in the horn of Africa because it only represented the first growing cycle in Fig. 7, where two vegetation growing cycles followed two rainy seasons (Zhang et al. 2005).

Interannual variation in GSL showed a considerable spatial difference across various climate regions. It was relatively small in cold and polar climate regions with a STD of generally less than 15 days. In contrast, the STD was larger than

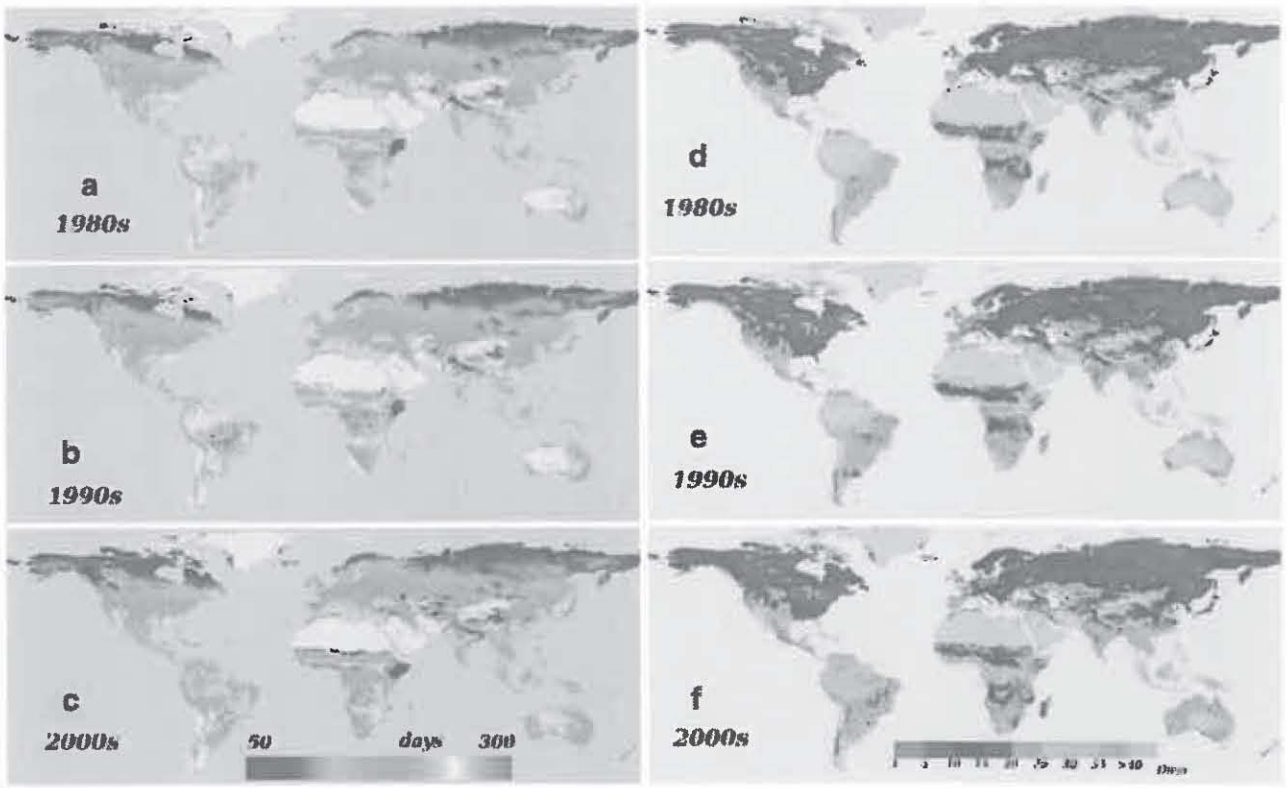

Fig. 7 Spatial pattern in average GSL (**a**, **b**, and **c**) and interannual standard deviation (**d**, **e**, and **f**). Note the first growing season is presented if there are multiple seasons within a year. *Gray* indicates no phenology detection

20 days in dry and tropical climate regimes. It was largest in tropical forests, where it could be more than 40 days.

Long-term trend in GSL

The GSL trend varies considerably with geographic and climate regions (Figs. 8, 9, and 10, Tables 3 and 4). In NA, significantly prolonged GSL was most prominently observed from 1982 to 2010 although GSL became shorter insignificantly in BS and Cs from 2000 to 2010 (Fig. 8 and Table 3). Particularly, GSL significantly increased consistently in Ds and ET during the past 30 years. This pattern was also reflected in pixel-based trends (Figs. 9 and 10). The proportion of pixels was 1–3 % for prolonged GSL in ET and Ds while it was less than 0.4 % for shortened GSL. In Df, prolonged GSL occurred in 11 % of the area from 1982 to 1999 and 4 % from 2000 to 2010, while shortened GSL appeared in 2 and 7 %, respectively. In other climate regions, the area that changed significantly was less than 1 %.

GSL tended to be short in most climate regions across Europe from 1982 to 2010. It was significantly shortened in Cs from 1982 to 2010 and Ds from 2000 to 2010 (Table 3). Although the proportion of pixels was small (<1 %), there were more pixels with shortened GSL than those with prolonged GSL from 1982 to 2010 in ET, Ds, Cs, and BS, respectively. In Df, shortened GSL appeared in 4 % (1982–1999) and 10 % (2000–2010) of area while prolonged GSL occurred in 6 and 3 %, respectively (Figs. 9 and 10).

Significantly prolonged GSL in Asia presented in BS (2000–2010), BW (2000–2010), and CS (1982–2010), while shortened GSL appeared in BS (1982–1999) and Df (2000–2010) (Table 3). The proportion of pixels with significant GSL shift was relatively large in Df and Dw while it was smaller than 1 % in other climate regions. In Df, it was 2 % (1982–1999) and 3 % (2000–2010) for prolonged GSL, and 3 % (1982–1999) and 7 % (2000–2010) for shortened GSL, respectively. In Dw, the proportion was 3, 3, 1, and 1 %, respectively.

In South America, GSL mainly showed opposite overall trends between 1982–1999 and 2000–2010 although the trends were not necessarily significant (Fig. 8 and Table 4). Significant opposite trends only occurred in Cf, where GSL increased (0.9 days/year) from 1982 to 1999 while it decreased (1.7 days/year) from 2000 to 2010. Moreover, the GSL could transit from positive to negative trends across different climate regions. Indeed, GSL presented a prolonged trend in dry climate (BS and BW) while it showed a shortened trend in temperate climate (Cf and Cw) from 2000 to 2010. In

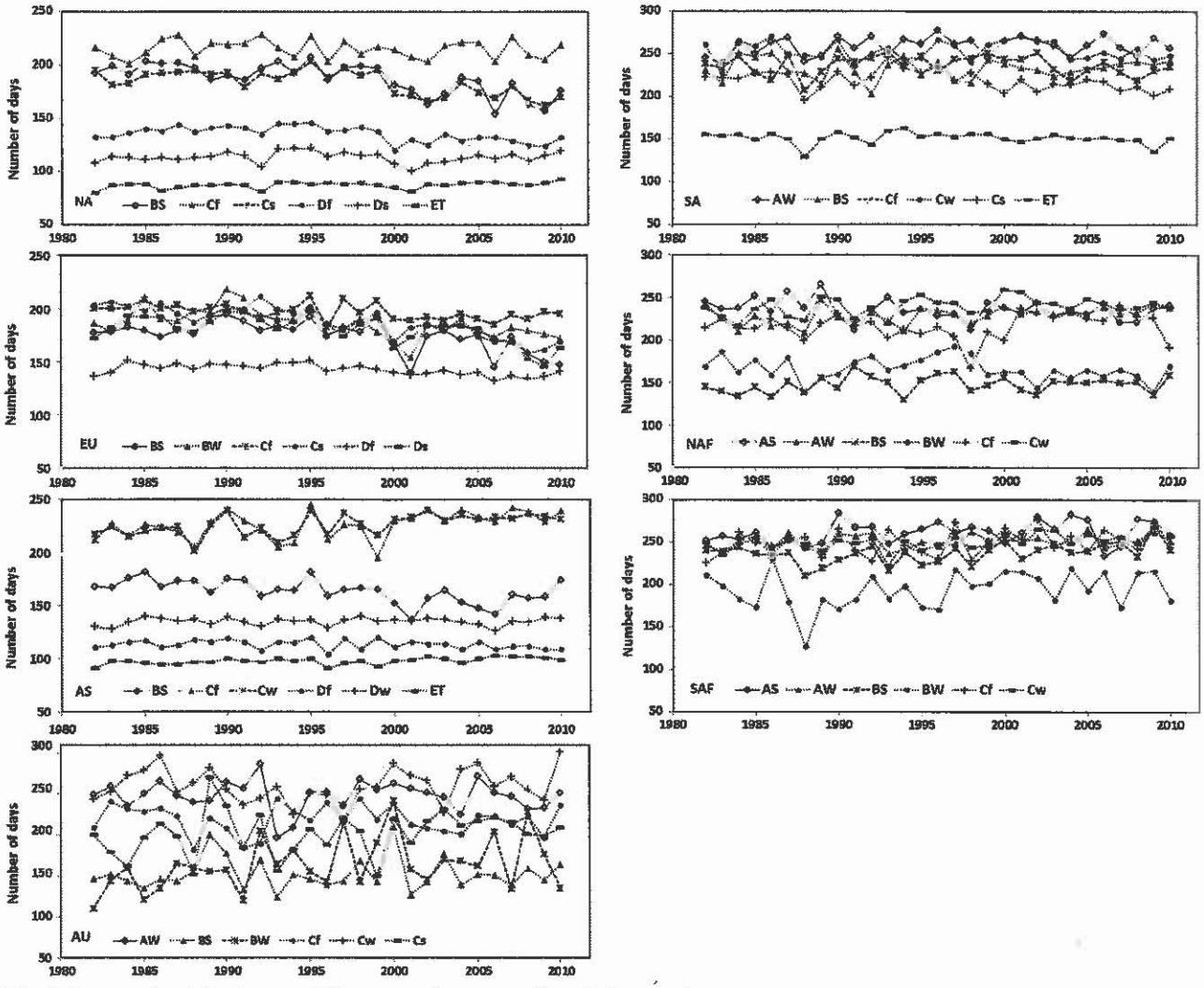

Fig. 8 Interannual variation in mean GSL across various geographic and climate regions

general, there were more pixels with reduced GSL than increased GSL in AW, Cf, and Cw from 1982 to 2010 (Figs. 9 and 10).

GSL was generally prolonged across the Sahelian and sub-Sahelian regions where AW, BS, and BW are dominated, although the significant overall trend only occurred in BS from 1982 to 1999 (Fig. 8 and Table 4). However, GSL reduced from 1982 to 2010 in As with a significantly shortened trend from 1982 to 1999. Overall, the proportion of pixels with prolonged GSL was larger than that with reduced GSL. It was 2–5 % for increased GSL in AW and BS from 1982 to 2010, while the proportion was less than 1 % for decreased GSL (Figs. 9 and 10). In As and BW, there were slightly more pixels with increased GSL than decreased GSL from 2000 to 2010 while the proportion for either shift directions was equivalent from 1982 to 1999.

In the Southern Hemisphere of Africa, the significant GSL trend only appeared in As from 1982 to 1999. However, the proportion of pixels with significant trends could be as large as 4 % in a climate region. The proportion for significantly reduced GSL was larger than that for prolonged GSL in AW, BS, BW, and Cw from 1982 to 1999, while this pattern was reversed from 2000 to 2010. As a result, the trend from 1982 to 2010 was generally insignificant.

In Australia, GSL presented an increased trend in BW (2.9 days/year) and a decreased trend in Cw (1.5 days/year) from 1982 to 1999. There were no significant trends across other climate regions during the two periods of 1982–1999 and 2000–2010. However, the proportion of pixels showing negative trends was larger than that for positive trends in AW and BW from 2000 to 2010, which was similar in both directions from 1982 to 1999 (Figs. 9 and 10). In BS, the proportion for prolonged GSL was larger than that for reduced GSL from 1982 to 2010 although it was larger than 2 % in both positive and negative trends. In other climate regions, the area with significant trends was very small (<1 %).

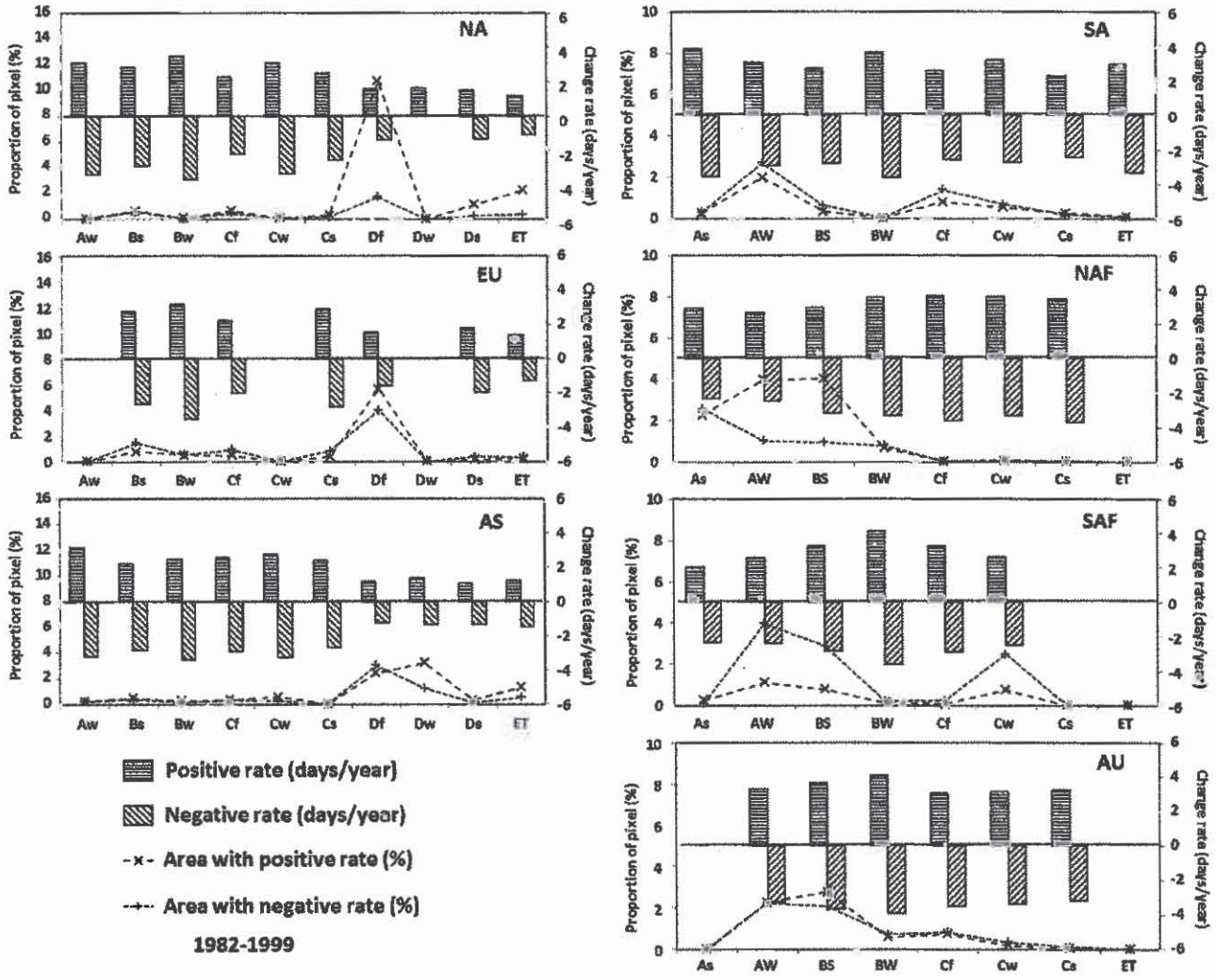

Fig. 9 The shift rate averaged from significant pixel-based trends ($P<0.1$) and the proportion of pixels with significant trends in growing seasonal length from 1982 to 1999

Discussion

A long-term global LSP dataset was produced from multiple-sensor satellite data in this study, however, to be aware of the limitation and quality that could improve our interpretation of the impacts of climate change on ecosystem dynamics. Although the abiotic noises caused by cloud cover and snow appearance were explicitly reduced in simulating temporal vegetative EVI2 trajectory, the uncertainties in the reconstructed EVI2 series are large if cloud cover is consistent during a vegetation growing season. Further, the annual EVI2 trajectories may not well reflect subtle seasonal cycles in some evergreen forests and shrublands. Thus, the retrieved phenological metrics are likely not so reliable as those from deciduous forests, croplands, and grasslands. Moreover, temporal MODIS data have a relatively higher quality than AVHRR data, and their continuity remains uncertain. As a result, these factors likely affect the phenological trend analysis from 1982 to 2010.

Validation is required to understand well the accuracy of long-term global LSP detections. It ensures the reliability of long-term trend and interannual variation of phenology in response to climate change. To validate the accuracy of phenology detection, sufficient field measurements comparable to a satellite footprint are needed. This requires the field data to reconcile with satellite-based phenological observations, which is currently extremely challenging. The validation effort will become more practical with the inclusion of observations from webcam (Richardson et al. 2009) and landscape measurements upscaled from field observations (Liang et al. 2011). However, such data are currently very limited for validating our global LSP product.

Comparison of the satellite-derived phenological trends from various studies could improve our understanding of the

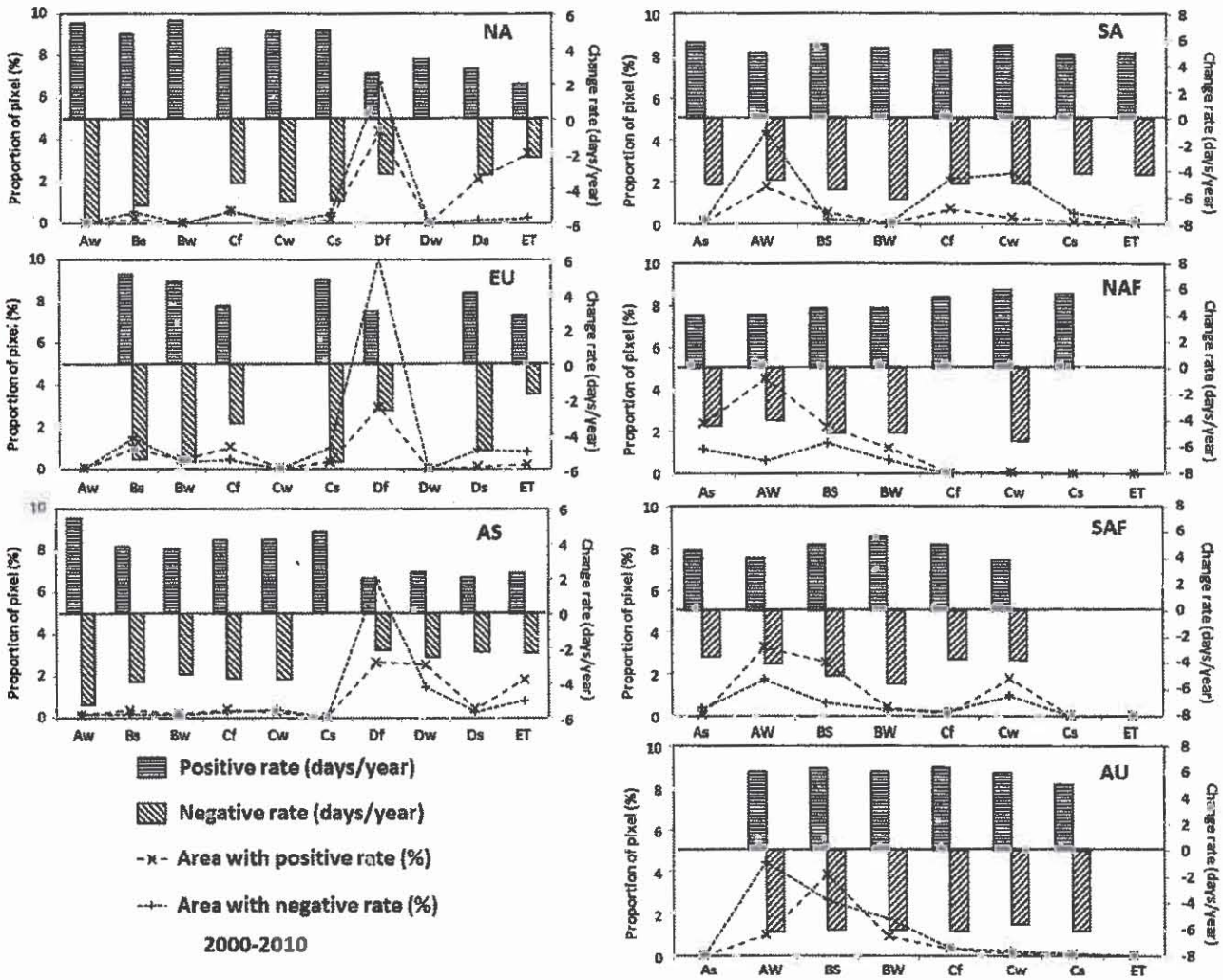

Fig. 10 The shift rate averaged from significant pixel-based trends ($P<0.1$) and the proportion of pixels with significant trends in growing seasonal length from 2000 to 2010

complexity in trend detections. The phenological trend and interannual variation vary greatly with the methods used to process the time series of satellite data. First, time series of NDVI and EVI2 are not temporally consistent, and EVI2 has

Table 3 Overall trend in the growing season length (days/year) in North America (NA), Europe (EU), and Asia (AS)

GSL		AW	BS	BW	Cf	Cw	Cs	Df	Dw	Ds	ET
NA	1982–1999	N/A	0.04	**1.14**	0.19	0.87	0.35	**0.38**	0.26	**0.43**	**0.25**
	2000–2010	N/A	−1.08	0.38	0.3	1.27	−0.37	0.25	0.65	**1.27**	**0.65**
EU	1982–1999	N/A	0.39	−0.41	−0.09	N/A	**−0.74**	0.14	N/A	0.16	−0.02
	2000–2010	N/A	−1.33	0.75	0.46	N/A	**−1.86**	−0.31	N/A	**−2.19**	0.55
AS	1982–1999	0.02	**−0.46**	0.28	−0.27	0.39	**1.04**	0.05	0.15	0.12	0.03
	2000–2010	−0.86	**1.63**	**0.57**	0.34	−0.03	**3.75**	**−0.44**	0.02	0.25	0.22

The bold value indicatesignificant trends (P value<0.1)

N/A not applicable, *GSL* length of vegetation growing season, *AW* tropical climate—dry winter, *BS* dry climate—steppe climate, *BW* dry climate—desert climate, *Cf* temperate climate—fully humid season, *Cw* temperate climate—dry winter, *Cs* temperate climate—dry summer, *Df* cold climate—fully humid season, *Dw* cold climate—dry winter, *Ds* cold climate—dry summer, *ET* polar climate—tundra

Table 4 Overall trend in the growing season length (days/year) in South America (SA), the Northern Hemisphere of Africa (NAF), the Southern Hemisphere of Africa (SAF), and Australia (AU)

GSL		As	AW	BS	BW	Cf	Cw	Cs	ET
SA	1982–1999	0.89	**0.8**	−0.36	0.15	**0.85**	0.01	0.35	0.3
	2000–2010	−0.75	−0.71	**0.87**	**1.61**	**−1.67**	**−2.39**	−0.41	−0.52
NAF	1982–1999	**−0.94**	0.18	**0.75**	0.66	**−1.26**	0.59	0.03	N/A
	2000–2010	−0.37	0.36	0.32	−0.07	−0.74	**−1.62**	−0.45	N/A
SAF	1982–1999	**0.96**	0.25	−0.35	0.26	0.13	0.03	−0.26	N/A
	2000–2010	0.04	0.23	0.83	−1.56	−0.79	0.06	−0.87	N/A
AU	1982–1999	N/A	−0.23	0	**2.86**	0.28	**−1.54**	−0.15	N/A
	2000–2010	N/A	−1.65	−1.54	−2.27	0.08	−0.18	−0.85	N/A

The bold value indicates significant trend (P value<0.1)

N/A not applicable, *GSL* length of vegetation growing season, *As* tropical climate—dry summer, *AW* tropical climate—dry winter, *BS* dry climate—steppe climate, *BW* dry climate—desert climate, *Cf* temperate climate—fully humid season, *Cw* temperate climate—dry winter, *Cs* temperate climate—dry summer, *ET* polar climate—tundra

advantages over NDVI in monitoring vegetation seasonal dynamics (Huete et al. 2006; Jiang et al. 2008; Rocha et al. 2008). Second, although the same phenological term is used for defining a phenological event, such as OGI, the corresponding biophysical meaning is different among various methods such as absolute threshold (e.g., Lloyd 1990; Fisher 1994; Myneni et al. 1997; Zhou et al. 2001), relative threshold (e.g., White et al. 1997; Jönsson and Eklundh 2002; Delbart et al. 2005; Karlsen et al. 2006), quadratic model (de Beurs and Henebry 2005a), moving average (Reed et al. 1994), change rate in NDVI (Moulin et al. 1997; Tateishi and Ebata 2004; Piao et al. 2006), and curvature change rate (Zhang et al. 2003). Third, temporal greenness trajectories reflected seasonal vegetation dynamics are always poorly reconstructed although various smoothing approaches have been developed. As a result, the OGI detected from various approaches differs as much as ±60 days (White et al. 2009). Fourth, the trend calculated from the average of phenologic metrics over a climate region is not exactly the same as that calculated from pixel-based metrics. Although the direction of the overall trend in a climate region follows the pixel-based trends in majority pixels, the statistical significance and magnitude of the overall trend are contributed from all pixels. As a result, the significance of overall trend in a climate region may not match well with significant pixel-based trends. With this in mind, we could understand better the discrepancy of phenological trends and interannual variations from various studies.

This study revealed that the early trend and magnitude of rate in OGI varied greatly with climate regions in middle–high latitudes. In polar climate, OGI came early and GSL was prolonged with significant trends in NA from 1982 to 2010, but no significant trends were found in Eurasia. In cold and temperate climates, there were more pixels with significantly early trends than those with late trends from 1982 to 1999, and early trends reduced from 2001 to 2010. It is likely that the impacts of warming climate on greenness increase were more consistent in polar climate than other climate regions. Moreover, our results in northern middle–high latitudes are generally comparable with some previous studies, but not with others. Based on AVHRR GIMMS from 1982 to 1999, the early shift rate in OGI was 0.36 days/year in Eurasia and 0.42 days/year in NA (Zhou et al. 2001), 0.25 days/year from 45° to 75°N (Tucker et al. 2001), 0.74 days/year in North China (Piao et al. 2006), and 0.31 days/year in the temperate Northern Hemisphere (de Jong et al. 2011). According to AVHRR PAL data, the early shift rate in OGI was 0.62 days/year in NA and 0.42 days/year in Europe from 1985 to 1999 (de Beurs and Henebry 2005a), 0.03 days/year in temperate climate from 2000 to 2008 (de Jong et al. 2011), and 0.54 days/year in Europe from 1982 to 2000 (Stöckli and Vidale 2004). Based on AVHHR GVIX (4 km) data, in NA from 1982 to 2005, OGI came early with a rate of 0.32 days/year from 40°N northward but delayed 0.24 days/year in 31.5°N southward (Zhang et al. 2007). In contrast, significant OGI trends were generally not found across NA according to biweekly AVHRR GIMMS data (8 km) from 1982 to 2003 (Reed 2006) and from 1982 to 2006 (White et al. 2009). Similarly, GSL derived from AVHRR GIMMS data showed an increased rate of 0.95 days/year in Eurasia and 0.63 days/year in NA (Zhou et al. 2001), 0.05 days/year from 45° to 75°N from 1982 to 1999 (Tucker et al. 2001), and 0.96 days/year in Europe from 1982 to 2000 (Stöckli and Vidale 2004).

In the dry climate of western NA, OGI, overall, showed no significant trend but GSL increased during 1982–1999. This is likely associated with the complex cycles in precipitation and dry season length during past decades (Groisman and Knight 2008; Zhang et al. 2010). In dry climate across Asia, GSL was significantly prolonged in BS and BW during the period of 2000–2010 although significant shortening occurred in BS

from 1982 to 1999. The positive trend is likely associated with the precipitation increase during the recent decade on the Tibetan Plateau (Piao et al. 2006; Shen et al. 2011). Moreover, our results also show that OGI presented no significant trends from 2000 to 2010 and that OGI shifted early in BW from 1982 to 1999. This complex pattern is comparable with previous results from GIMMS data which indicates that an early GIMMS OGI trend (0.38 days/year) appeared from 1982 to 1999 (Shen et al. 2011).

In South America, OGI showed a late trend during the last 3 decades particularly from 1982 to 1999. Correspondingly, GSL decreased 1–15 days in tropical and temperate climates from the 1990s to the 2000s although it increased from the 1980s to the 1990s. This reduction during the 2000s is consistent with the finding of NPP (net primary productivity) reduction because of drought impacts induced from warming temperature (Zhao and Running 2010).

The early OGI trend and prolonged GSL in the Northern Hemisphere of Africa were evident from 1982 to 1999; however, the rate reduced or converted to the opposite directions during 2000–2010. This pattern is generally consistent with previous studies (Olsson et al. 2005; Heumann et al. 2007; Vrieling et al. 2013). The trend is likely related to the increase of rainfall during 1980s to the 1990s as well as land use change (Olsson et al. 2005). But the result is discrepant with that from GIMMS AVHRR NDVI during 1982–2003. The latter indicates that shortened GSL was dominant from 1982 to 2003 (Julien and Sobrino 2009).

The overall insignificant GSL change (but more pixels with significant increases than decreases) in the Southern Hemisphere of Africa from 2000 to 2010 is discrepant with the decreased trend of NPP as described by Zhao and Running (2010). However, the insignificant trend from 1982 to 2010 in this study is similar to the results of GIMSS data during 1982–2011 (Vrieling et al. 2013) and 1982–2006 (de Jong et al. 2011) where pixels with significantly increased and decreased trends were sparsely distributed across the region.

Conclusions

We investigated interannual variations and trends of LSP from 1982 to 2010 over individual climate regions globally. The seasonal vegetative greenness was simulated from long-term EVI2 time series after snow and cloud effects were explicitly reduced. Phenological metrics were retrieved from PLM-LSPD which provides a flexible, repeatable, and realistic means to monitor seasonal and interannual dynamics in vegetation across the globe. Because frequent cloud cover during a vegetation growing season strongly limits the reconstruction of a vegetation growing cycle, the proportion of good observations provides the overall reliability of phenology detection in individual pixels. On the other hand, the quality of phenology retrieval could vary with ecosystem types. Since the annual EVI2 cycle is more complex and less distinguishable in drylands and evergreen forests than that in other ecosystems, the retrieved phenological metrics likely contain relatively high uncertainty. Thus, it is urgently needed to develop robust methods to validate and assess the accuracy of long-term LSP detections and the phenological trends across various ecosystems.

The spatial patterns in OGI and GSL were very similar during the last 3 decades because they were mainly controlled by global climate patterns. However, interannual variation in phenology was larger in tropical and dry climates than in cold and polar climate regions. This is likely attributed to the difference in the seasonal variation between temperature and precipitation. Temperature seasonality is generally regular interannually, which leads to the low variability in vegetation phenology in middle–high latitudes. In contrast, rainfall seasonality is relatively more variable, which results in the high variability of interannual OGI and GSL in dry climate and seasonal dry tropical regions.

The phenological trend and interannual variation exhibited great variability across geographic and climatic regions. OGI generally shifted early and GSL was prolonged from 1982 to 2010 in temperate, cold, and polar climates in the North Hemisphere although the trends were not necessarily significant in individual climate regions and the proportion of pixels with significant trends was generally less than 10 %. However, the pixels with significantly advanced OGI reduced during 2000–2010 relative to those from 1982 to 1999, and the significant trends were more evident in North America and Asia than those in Europe. In precipitation-controlled dry climate over the Northern Hemisphere, OGI and GSL presented no significant trends in Europe and western NA (except increased GSL in BW of NA) while GSL was mostly prolonged in Asia from 2000 to 2010. In South America, late OGI was consistent, particularly, from 1982 to 1999 while GSL varied between the periods of 1982–1999 and 2000–2010, where GSL significantly reduced in temperate climate but increased in dry climate from 2000 to 2010. No significant OGI trend was found, but prolonged GSL was evident over individual climate regions in the Northern Hemisphere of Africa during the last 3 decades because there were more pixels with significantly early OGI and increased GSL than those with late OGI and shortened GSL. OGI in the Southern Hemisphere of Africa mainly showed late trends, and the proportion of pixels with reduced GSL trends was larger than that for prolonged trends from 1982 to 1999, but it was reversed from 2000 to 2010. In Australia, GSL exhibited considerable interannual variation, but the consistent trend lacked presence in most regions.

The combination of the overall trend and pixel-based trend provides phenological characteristics varying at different spatial scales in a climate region. This could improve our

Liang L, Schwartz MD, Fei S (2011) Validating satellite phenology through intensive ground observation and landscape scaling in a mixed seasonal forest. Remote Sens Environ 115:143–157

Lloyd D (1990) A phenological classification of terrestrial vegetation cover using shortwave vegetation index imagery. Int J Remote Sens 11:2269–2279

Lotsch A, Friedl MA, Anderson BT, Tucker CJ (2003) Coupled vegetation-precipitation variability observed from satellite and climate records. Geophys Res Lett 30(14). doi:10.1029/2003GL017506

Moulin S, Kergoat L, Viovy N, Dedieu G (1997) Global-scale assessment of vegetation phenology using NOAA/AVHRR satellite measurements. J Climate 10(6):1154–1170

Myneni RB, Keeling CD, Tucker CJ, Asrar G, Nemani RR (1997) Increased plant growth in the northern high latitudes from 1981–1991. Nature 386:698–702

Olson DM, Dinerstein E, Wikramanayake ED, Burgess ND, Powell GVN, Underwood EC, D'Amico JA, Itoua I, Strand HE, Morrison JC, Loucks CJ, Allnutt TF, Rick-etts TH, Kura Y, Lamoreux JF, Wettengel WW, Hedao P, Kassem KR (2001) Terrestrial ecoregions of the world: a new map of life on Earth. Bioscience 51(11):933–938

Olsson L, Eklundh L, Ardö J (2005) Greening of the Sahel—trends, patterns and hypotheses. J Arid Environ 63:556–566

Pedelty J, Vermote EF, Devadiga S, Roy D, Schaaf C, Privette J et al (2007) Generating a long-term land data record from the AVHRR and MODIS instruments. Geoscience and Remote Sensing Symposium, 2007. IGARSS 2007. IEEE International. pp 1021–1025

Piao S, Fang J, He J (2006) Variations in vegetation net primary production in the Qinghai-Xizang Plateau, China, from 1982 to 1999. Clim Chang 74(1):253–267

Reader R, Radford JS, Lieth H (1974) Modeling important phytophenological events in eastern North America. In: Lieth H (ed) Phenology and Seasonality Modeling. Springer, New York, pp 329–342

Reed BC (2006) Trend analysis of time-series phenology of North America derived from satellite data. GIsci Remote Sens 43(1):24–38

Reed BC, Brown JF, VanderZee D, Loveland TR, Merchant JW, Ohlen DO (1994) Measuring phenological variablity from satellite imagery. J Veg Sci 5:703–714

Richardson AD, Bailey AS, Denny EG, Martin CW, O'Keefe J (2006) Phenology of a northern hardwood forest canopy. Glob Chang Biol 12:1174–1188

Richardson AD, Braswell BH, Hollinger D, Jenkins JP, Ollinger SV (2009) Near-surface remote sensing of spatial and temporal variation in canopy phenology. Ecol Appl 19(6):1417–1428

Rocha AV, Shaver GR (2009) Advantages of a two band EVI calculated from solar and photosynthetically active radiation fluxes. Agric For Meteorol 149(9):1560–1563

Rocha AV, Potts DL, Goulden ML (2008) Standing litter as a driver of interannual CO2 exchange variability in a freshwater marsh. J Geophys Res 113, G04020. doi:10.1029/2008JG000713

Shen M, Tang Y, Chen J, Zhu X, Zheng Y (2011) Influences of temperature and precipitation before the growing season on spring phenology in grasslands of the central and eastern Qinghai-Tibetan Plateau. Agric For Meteorol 151:1711–1722

Sparks TH, Carey PD (1995) The responses of species to climate over 2 centuries—an analysis of the Marsham phonological record, 1736–1947. J Ecol 83:321–329

Stöckli R, Vidale P (2004) European plant phenology and climate as seen in a 20-year AVHRR land-surface parameter dataset. Int J Remote Sens 25(17):3303–3330. doi:10.1080/01431160310001618149

Stowe LL, Davis PA, McClain EP (1999) Scientific basis and initial evaluation of the CLAVR-1 global clear cloud classification algorithm for Advanced Very High Resolution Radiometer. J Atmos Ocean Technol 16:656–681

Tateishi R, Ebata, M (2004) Analysis of phenological change patterns using 1982–2000 Advanced Very High Resolution Radiometer (AVHRR) data. Int J Remote Sens 25:2287–2300

Tsend-Ayush J, Miura T, Didan K, Barreto-munoz A (2012) Compatibility analysis of Spot-4 vegetation and terra modis vegetation index products for long-term data records. Proceedings of IEEE international geoscience and remote sensing symposium, 22–27 July 2012, Munich, Germany

Tucker CJ, Slaback DA, Pinzon JE et al (2001) Higher northern latitude normalized difference vegetation index and growing season trends from 1982 to 1999. Int J Biometeorol 45:184–190

Tucker CJ, Pinzon JE, Brown ME, Slayback D, Pak EW, Mahoney R, Vermote E, Saleous N (2005) An extended AVHRR 8-km NDVI data set compatible with MODIS and SPOT Vegetation NDVI data. Int J Remote Sens 26(20):4485–4498

Vermote EF, Kaufman YJ (1995) Absolute calibration of AVHRR visible and nearinfrared channels using ocean and cloud views. Int J Remote Sens 16(13):2317–2340

Vrieling A, de Leeuw J, Said MY (2013) Length of growing period over Africa: variability and trends from 30 years of NDVI time series. Remote Sens 5:982–1000. doi:10.3390/rs5020982

White MA, Thornton PE, Running SW (1997) A continental phenology model for monitoring vegetation responses to interannual climatic variability. Glob Biogeochem Cycles 11:217–234

White MA, Hoffman F, Hargrove WW (2005) A global framework for monitoring phenological responses to climate change. Geophys Res Lett 32:1–4

White MA, de Beurs KM, Didan K, Inouye DW, Richardson AD, Jensen OP, O'Keefe J, Zhang G, Nemani RR, van Leeuwen WJD, Brown JF, de Wit A, Schaepman M, Lin XM, Dettinger M, Bailey AS, Kimball J, Schwartz MD, Baldocchi DD, Lee JT, Lauenroth WK (2009) Intercomparison, interpretation, and assessment of spring phenology in North America estimated from remote sensing for 1982–2006. Glob Chang Biol 15:2335–2359

Yoshioka H, Miura T, Obata K (2012) Derivation of relationships between spectral vegetation indices from multiple sensors based on vegetation isolines. Remote Sens 4:583–597. doi:10.3390/rs4030583

Zhang X, Friedl MA, Schaaf CB, Strahler AH, Hodges JCF, Gao F, Reed BC, Huete A (2003) Monitoring vegetation phenology using MODIS. Remote Sens Environ 84:471–475

Zhang X, Friedl MA, Schaaf CB, Strahler AH, Liu Z (2005) Monitoring the response of vegetation phenology to precipitation in Africa by coupling MODIS and TRMM instruments. J Geophys Res Atmos 110, D12103. doi:10.1029/2004JD005263

Zhang X, Friedl MA, Schaaf CB (2006) Global vegetation phenology from MODIS: evaluation of global patterns and comparison with in situ measurements. J Geophys Res 111, G04017. doi:10.1029/2006JG000217

Zhang X, Tarpley D, Sullivan J (2007) Diverse responses of vegetation phenology to a warming climate. Geophys Res Lett 34, L19405

Zhang X, Friedl MA, Schaaf CB (2009) Sensitivity of vegetation phenology detection to the temporal resolution of satellite data. Int J Remote Sens 30(8):2061–2074. doi:10.1080.01431160802549237

Zhang X, Goldberg M, Tarpley D, Friedl M, Morisette J, Kongan F, Yu Y (2010) Drought-induced vegetation reduction in southwestern North America. Environ Res Lett 5:024008. doi:10.1088/1748-9326/5/2/024008

Zhao M, Running SW (2010) Drought-induced reduction in global terrestrial net primary production from 2000 through 2009. Science 329:940–943

Zhou L, Tucker CJ, Kaufmann RK, Slayback D, Shabanov NV, Myneni RB (2001) Variation in northern vegetation activity inferred from satellite data of vegetation index during 1981 to 1999. J Geophys Res 106(D17):20069–20083

Zhu K, Yuan M (1963) A productive science—phenology. Public Science, No 1

understanding of the phenological response to climate change. However, future research is needed to explore how trends (including significance, magnitude, and direction) in individual pixels affect the overall trend in a climate region and why positive and negative trends coexist in the same climate region.

Moreover, the trend was conservatively analyzed by separating the two periods of 1982–1999 and 2000–2010 because of the different qualities and some inconsistencies between AVHRR LTDR and MODIS CMG. In this case, the direction of the overall trend in a climate region from 1982 to 2010 is suggested to follow the direction that consistently occurred in both periods. However, it was uncertain if the trend direction was opposite during these two periods. As a result, further evaluation and calibration of the EVI2 time series derived from AVHRR LTDR and MODIS CMG could enable us to provide more reliable long-term phenological variation and trends.

Finally, the trends of vegetation phenology during the last 3 decades were substantially variable and inconsistent in most parts of the globe. To understand the complex responses of long-term phenology to climate change, it is our ongoing efforts to examine the correlation between phenologic metrics and climate variables at individual climate regions globally.

Acknowledgments This work was partially supported by NASA MEaSUREs contract NNX08AT05A. We wish to thank Kamel Didan and Armando Barreto Munoz at the University of Arizona for providing long-term EVI2 detest.

References

Ahl DE, Gower ST, Burrows SN, Shabanov NV, Myneni RB, Knyazikhin Y (2006) Monitoring spring canopy phenology of a deciduous broadleaf forest using MODIS. Remote Sens Environ 104(1):88–95

Chen X, Hu B, Yu R (2005) Spatial and temporal variation of phenological growing season and climate change impacts in temperate eastern China. Glob Chang Biol 11:1118–1130

de Beurs KM, Henebry GM (2004) Land surface phenology, climatic variation, and institutional change: analyzing agricultural land cover change in Kazakhstan. Remote Sens Environ 89:497–509

de Beurs KM, Henebry GM (2005a) A statistical framework for the analysis of long image time series. Int J Remote Sens 26(8):1551–1573

de Beurs KM, Henebry GM (2005b) Land surface phenology and temperature variation in the IGBP high-latitude transects. Glob Chang Biol 11:779–790

de Jong R, de Bruin S, de Wit A, Schaepman ME, Dent DL (2011) Analysis of monotonic greening and browning trends from global NDVI time-series. Remote Sens Environ 115:692–702

Delbart N, Kergoat L, Le Toan T, Lhermitte J, Picard G (2005) Determination of phenological dates in boreal regions using normalized difference water index. Remote Sens Environ 97:26–38

Eidenshink JC (1992) The 1990 conterminous U.S. AVHRR data set. Photogramm Eng Remote Sens 58(6):809–813

Fisher A (1994) A model for the seasonal variations of vegetation indices in coarse resolution data and its inversion to extract crop parameters. Remote Sens Environ 48:220–230

Fisher JI, Mustard JF, Vadeboncoeur MA (2006) Green leaf phenology at Landsat resolution: scaling from the field to the satellite. Remote Sens Environ 100:265–279

Friedl MA, Henebry G, Reed B et al (2006) Land surface phenology: a community white paper requested by NASA.ftp://ftp.iluci.org/Land_ESDR/Phenology_Friedl_whitepaper.pdf

Groisman PYA, Knight RW (2008) Prolonged dry episodes over the conterminous United States: new tendencies emerging during the last 40 years. J Clim 21:1850–1862

Hargrove WW, Spruce JP, Gasser GE, Hoffman FM (2009) Toward a national early warning system for forest disturbances using remotely sensed canopy phenology. Photogramm Eng Remote Sens 75:1150–1156

Heumann W, Seaquist JW, Eklundh L, Jonsson P (2007) AVHRR derived phenological change in the Sahel and Soudan, Africa, 1982–2005. Remote Sens Environ 108(4):385–392

Hopkins AD (1938) Bioclimatics—a science of life and climate relations. US Department of Agriculture Misc. Publication No. 280. US Government Printing Office, Washington, DC

Huete AR, Didan K, Miura T, Rodriguez EP, Gao X, Ferreira LG (2002) Overview of the radiometric and biophysical performance of the MODIS vegetation indices. Remote Sens Environ 83:195–213

Huete AR, Didan K, Shimabukuro YE, Ratana P, Saleska CR, Hutyra LR et al (2006) Amazon rainforests green-up with sunlight in dry season. Geophys Res Lett 33, L06405. doi:10.1029/2005GL025583

IPCC (2007) Climate change 2007: impacts, adaptation, and vulnerability contribution of working group II to the fourth assessment report of the Intergovernment Panel on Climate Change, ed M L Parry, O F Canziani, J P Palutikof, P J van der Linden and C E Hanson (Cambridge: CambridgeUniversity Press) 976 pp

James ME, Kalluri SNV (1994) The Pathfinder AVHRR land data set: an improved coarse resolution data set for terrestrial monitoring. Int J Remote Sens Special Issue on Global Data Sets 15(17):3347–3363

Jiang Z, Huete AR, Didan K, Miura T (2008) Development of a two-band enhanced vegetation index without a blue band. Remote Sens Environ 112:3833–3845

Jönsson P, Eklundh L (2002) Seasonality extraction by function fitting to time-series of satellite sensor data. IEEE T Geosci Remote 40:1824–1831

Julien Y, Sobrino JA (2009) Global land surface phenology trends from GIMMS database. Int J Remote Sens 30(13):3495–3513

Justice CO, Vermote E, Townshend JRG et al (1997) The Moderate Resolution Imaging Spectroradiometer (MODIS): land remote sensing for global change research. IEEE Trans Geosci Remote Sens 36:1228–1249

Karlsen SR, Elvebakk A, Høgda KA, Johansen B (2006) Satellite based mapping of the growing season and bioclimatic zones in Fennoscandia. Glob Ecol Biogeogr 15:416–430

Kim Y, Huete AR, Miura T, Jiang Z (2010) Spectral compatibility of vegetation indices across sensors: band decomposition analysis with Hyperion data. J Appl Remote Sens 4:043520

Kogan F, Gitelson A, Zakarin E, Spivak L, Lebed L (2003) AVHRR-based spectral vegetation index for quantitative assessment of vegetation state and productivity: calibration and validation. Photogramm Eng Remote Sens 69(8):899–906

Kovalskyy V, David P, Roy DP, Zhang X, Ju J (2012) The suitability of multi-temporal web-enabled Landsat data NDVI for phenological monitoring—a comparison with flux tower and MODIS NDVI. Remote Sens Lett 3(4):325–334

Lauscher F (1978) Neue Analysen ältester und neuerer phänologischer Reihen. Arch Met Geophysik Klimatol (B) 26:373–385